Energy & Environmental Science

Cite this: *Energy Environ. Sci.*, 2012, **5**, 9595

www.rsc.org/ees

PAPER

Facile synthesis of $Li_4Ti_5O_{12}$/C composite with super rate performance†

Baohua Li,[a] Cuiping Han,[ab] Yan-Bing He,[a] Cheng Yang,[a] Hongda Du,[a] Quan-Hong Yang*[ac] and Feiyu Kang*[ab]

Received 19th June 2012, Accepted 16th August 2012
DOI: 10.1039/c2ee22591c

The $Li_4Ti_5O_{12}$/C composite with lump morphology and excellent rate performance are synthesized using a facile hydrothermal method followed by a low temperature heat treatment. In the hydrothermal process, the introduction of cetyltrimethylammonium bromide (CTAB) as a surfactant significantly improves the rate performance of $Li_4Ti_5O_{12}$/C composite as anode material for lithium ion battery (LIB). The specific capacities of the obtained composite at charge and discharge rates of 0.1, 1, 5, 10 and 20 C are 176, 163, 156, 151 and 136 mA h g^{-1}, respectively, which is apparently larger than those of the $Li_4Ti_5O_{12}$/C free from CTAB in the preparation. The $Li_4Ti_5O_{12}$/C prepared in presence of CTAB also shows excellent cycling performance at high rate, which is attributed to its larger diffusion coefficient of lithium ion (6.82×10^{-12} cm^2 s^{-1}) and smaller charge-transfer resistance (R_{ct}) (19.2 Ω) than those of the composite (1.22×10^{-13} cm^2 s^{-1} and 50.2 Ω) free from CTAB in the preparation. The $Li_4Ti_5O_{12}$ particles obtained in presence of CTAB are coated uniformly by a thin carbon layer with a thickness of ~1 nm, whereas the $Li_4Ti_5O_{12}$ particles obtained in absence of CTAB are covered by relatively thick surface layers with a thickness of ~2.5 nm, which is too thick, blocks the lithium ion diffusion and leads to low ionic conductivity.

High power performance and long cycle life are essential to the lithium ion batteries (LIBs) technology, which is one of the key issues for solving the energy crisis such as for powering automotive vehicles, *etc.*[1–3] Efficient electrode materials are the hard core for the performance improvement of lithium ion battery. Among the potential anode materials for LIBs, the cubic spinel lithium titanate ($Li_4Ti_5O_{12}$) has attracted much attention recently.[4] Known as the "zero strain" lithium insertion host, $Li_4Ti_5O_{12}$ undergoes extremely small expansion and contraction during charge–discharge cycling,[5–7] and has a stable voltage plateau at approximately 1.5 V *versus* Li^+/Li, which is above the potential range where most types of electrolytes or solvents are reduced.[8–10] Additionally, its spinel framework provides 3-D network channels for fast lithium ion diffusion,[11] and $Li_4Ti_5O_{12}$ thus exhibits excellent lithium ion intercalation/deintercalation reversibility and structural stability, and can effectively avoid the

[a]*Key Laboratory of Thermal Management Engineering and Materials, Graduate School at Shenzhen, Tsinghua University, Shenzhen 518055, China. E-mail: yang.quanhong@mail.sz.tsinghua.edu.cn*
[b]*Laboratory of Advanced Materials, Department of Materials Science and Engineering, Tsinghua University, Beijing 100084, China. E-mail: fykang@mail.tsinghua.edu.cn*
[c]*School of Chemical Engineering and Technology, Tianjin University, Tianjin 300072, China. E-mail: qhyangcn@tju.edu.cn*

† Electronic supplementary information (ESI) available: TG curves of the prepared $Li_4Ti_5O_{12}$/C; charge and discharge curves of $Li_4Ti_5O_{12}$/C with CTAB concentration of 6.5 g L^{-1}. See DOI: 10.1039/c2ee22591c

Broader context

Cubic spinel $Li_4Ti_5O_{12}$ shows increasing promise as a suitable anode material for high-power lithium ion batteries (LIB) due to its excellent cycling performance, structural and thermal stability. Unfortunately, very low intrinsic electronic conductivity and lithium-ion diffusion coefficient results in the poor high-rate charge–discharge capabilities of $Li_4Ti_5O_{12}$. In the past years, nanostructured or conductive carbon coated $Li_4Ti_5O_{12}$ materials with improved rate capability have been successfully prepared using various approaches. Most of these materials exhibit relatively low tap density and high irreversible capacity loss. In this work, the introduction of cetyltrimethyl ammonium bromide (CTAB) as a cationic surfactant in the hydrothermal process results in a successful preparation of $Li_4Ti_5O_{12}$/C composite which is characterized by a significantly improved rate performance. The obtained composite has specific capacities at 10 and 20 C as high as 151 and 136 mA h g^{-1}, respectively, but with unique nonporous lump-like morphology which indicates high tap density. Such super rate performance is supported by a much larger ion diffusion coefficient and less charge-transfer resistance as compared to the composite prepared in absence of CTAB. This material is expected to find practical application in high power LIB.

reduction of electrolyte on the surface of the electrode, which results in the formation of a solid electrolyte interface (SEI) film. Therefore, $Li_4Ti_5O_{12}$ has a significant promise for high-rate LIBs application.

Despite its advantages as presented above $Li_4Ti_5O_{12}$ shows low electronic conductivity ($<10^{-9}$ S cm^{-1}), which leads to poor high rate performance in the application as electrode material in LIBs. In order to improve the rate performance of $Li_4Ti_5O_{12}$ based electrode materials, various nanostructured $Li_4Ti_5O_{12}$ such as mesoporous microsphere,[12] hollow microsphere,[13] flower-like nanosheets,[14] sawtooth-like nanosheets,[15] nanostructured spherical particles,[16] hierarchical structures[17] have been successfully prepared. Carbon nanostructures, such as carbon nanotubes, graphene and amorphous carbon thin layers, are also introduced into $Li_4Ti_5O_{12}$ to obtain composite electrode materials.[18–25] These prepared materials show good rate charge and discharge performances due to their very large reaction areas with the electrolyte. However, these materials also show apparent drawbacks that are very low tap density and high irreversible capacity loss. For power LIBs, the volumetric energy density is even more significant than the mass energy density in the real applications. For most of nanostructured and composite $Li_4Ti_5O_{12}$ materials, it is very difficult to assemble commercial power batteries with high volumetric energy density. Thus, the synthesis of high tap density spinel $Li_4Ti_5O_{12}$ with excellent rate performance is urgently required to obtain a high performance density battery.

In this work, we report a novel $Li_4Ti_5O_{12}$ with lump morphology and super rate performance, which is prepared by a hydrothermal process followed by low temperature heat treatment. In this hydrothermal preparation possess, a tertiary ammonium surfactant, cetyltrimethyl ammonium bromide ($C_{16}H_{33}(CH_3)_3NBr$, abbreviated as CTAB) was introduced, which not only functions as a surfactant to restrain the growth of $Li_4Ti_5O_{12}$ particles, but also acts as a carbon source. Table 1 presents the high rate charge and discharge performance of $Li_4Ti_5O_{12}$ or $Li_4Ti_5O_{12}$/C composite with special morphology and structure (such as porous, mesoporous and hierarchically porous structure) prepared using a hydrothermal method in recent studies. It is seen that the discharge capacity of our prepared $Li_4Ti_5O_{12}$/C with a cubic structure at 10 and 20 C is amongst the largest capacity values ever reported for $Li_4Ti_5O_{12}$ or $Li_4Ti_5O_{12}$/C with a porous structure or designed nanostructure. We believe that this material has a great practical application value in both the power and energy storage lithium ion batteries.

Experimental

Synthesis of spinel $Li_4Ti_5O_{12}$/C

CTAB aqueous solution (~13 g L^{-1}) was prepared at ambient temperature (~298 K) with the deionized water under continuous stirring for 2 h. 10 mmol tetrabutyl titanate ($Ti(OC_4H_9)_4$) was added stepwise into 40 mL CTAB solution at ambient temperature under magnetic stirring (~3 h) and a yellow turbid liquid was obtained. At the same time, 9 mmol lithium acetate was dissolved in 5 mL purified water and after fully hydrolysis the lithium acetate solution was added to the above suspension liquid. The mixture was then transferred into a 60 mL Teflon-lined stainless steel autoclave and maintained at 180 °C for 48 h. White precipitate was obtained after the hydrothermal treatment. After drying in an oven at 85 °C, the as-prepared material was finally calcined at 700 °C for 7 h in argon filled atmosphere. For comparison, we also prepared the $Li_4Ti_5O_{12}$/C material using the same procedure without the addition of CTAB.

Sample characterization

The structure and phase composition of the obtained samples were characterized by X-ray diffraction measurement (XRD, Rigaku D/max 2500/PC using CuKα radiation with λ = 1.5418 Å) and the diffraction data were collected at a step mode over the angular range of 10–90°. The microstructure and morphologies of the prepared samples were characterized with field emission scanning electron microscopy (FE-SEM, HITACH S4800) at 10 kV and transmission electron microscopy (TEM, TECNAI G20) at an accelerating voltage of 200 kV. Raman measurement was performed with a Raman Spectrometer (Renishaw Invia Reflex, Britain) with a 514 nm Ar-ion laser.

Electrochemical characterization

Rate and cycling performance were carried out by galvanostatic testing CR2032-type coin cells assembled in an argon filled glove box (Mbraum). The coin cells used the prepared $Li_4Ti_5O_{12}$ as the cathode material, lithium foil as the anode, and polypropylene (Celgard 2500, Celgard Inc., USA) as the separator. The prepared $Li_4Ti_5O_{12}$, Acetylene Black and polyvinylidene fluoride (PVDF) binder were mixed homogeneously in a weight ratio of 80 : 10 : 10 and dissolved in *N*-methyl-2-pyrrolidinone (NMP) solvent. The formed slurry was uniformly coated on a copper foil current collector and dried under vacuum at 110 °C for 10 h. The electrolyte employed was 1 M $LiPF_6$ solution in ethylene

Table 1 High rate charge and discharge performance of $Li_4Ti_5O_{12}$ or $Li_4Ti_5O_{12}$/C prepared using the hydrothermal or solvothermal approach (herein, LTO represents $Li_4Ti_5O_{12}$)

Sample	Preparation method	10 C capacity (mA h g^{-1})	20 C capacity (mA h g^{-1})
Cubic LTO/C (this work)	Hydrothermal	151	136
Mesoporous LTO-C[12]	Solvothermal	~140	125.4
Hollow microsphere[13]	Hydrothermal	151	145
Hierarchically porous[17]	Hydrothermal	133.7 (1.5Ag^{-1})	128 (2 A g^{-1})
MWNT@LTO[20]	Hydrothermal	136.3	123.6
Porous LTO coated with N-doped carbon[26]	Heat treatment	129	/
LTO-600 (ref. 27)	Hydrothermal	~130	~110

carbonate and diethyl carbonate (EC–DEC) (volume ratio: 1 : 1). The assembled cells were galvanostatically charged and discharged under different current densities between 1.0 and 2.5 V using a Land 2001A battery testing system at room temperature. The electrochemical impedance spectrum (EIS) of the assembled cells was measured by using an electric IM6ex impedance analyzer in the frequency range of 10^{-2} to 10^{5} Hz. Impedance was measured at half state of the charge by applying a 5 mV ac oscillation. A cyclic voltammetry (CV) experiment was carried out with a VMP3 multichannel electrochemical station at a scan rate of 0.1 mV s^{-1} in the range of 0–2.5 V *vs.* Li^+/Li.

Results and discussion

Synthesis

As a cationic surfactant, CTAB has been used as a key toolbox for the facile preparation of some important nanocrystals,[28] *e.g.* gold nanorods and multipods;[29–31] it has also been used for the synthesis of some functional nanomaterials in the energy field, such as $LiFePO_4$ nanoparticles,[32] porous $ZnCo_2O_4$ nanowires,[33] hollow Sb nanoparticles,[34] and 3D dendritic TiO_2 nanostructures.[35]

CTAB is also used as the surfactant in this study. As schematically represented in Fig. 1a, when $Ti(OC_4H_9)_4$ is introduced stepwise into the CTAB solution, the $Ti(OC_4H_9)_4$ drop is instantly surrounded by CTA^+, and then is hydrolyzed to form the $Ti(OH)_4$. After the hydrothermal treatment, $Ti(OH)_4$ changed to anatase TiO_2 (proved by following XRD patterns). The Li ions are distributed uniformly around the anatase TiO_2 particles which were wrapped up by sticky organic compounds such as the hydrolysis products and the long chain surfactant. Then during the calcination treatment, Li ions react with TiO_2 quickly. Meanwhile, the organic compounds were decomposed and the residual amorphous carbon was coated around $Li_4Ti_5O_{12}$. Thus, the hydrothermal products can be transferred to $Li_4Ti_5O_{12}$/C after calcination at 700 °C for only 7 h which is much shorter than the normal cases. As discussed below, for the process free from the CTAB, it can be found that the particle size of $Ti(OH)_4$ and anatase TiO_2 is larger than that with CTAB, which is due to the fact that CTAB as a surfactant is adsorbed on the surface of $Ti(OH)_4$ particles as soon as $Ti(OC_4H_9)_4$ is hydrolysed and thus restrains their growth.

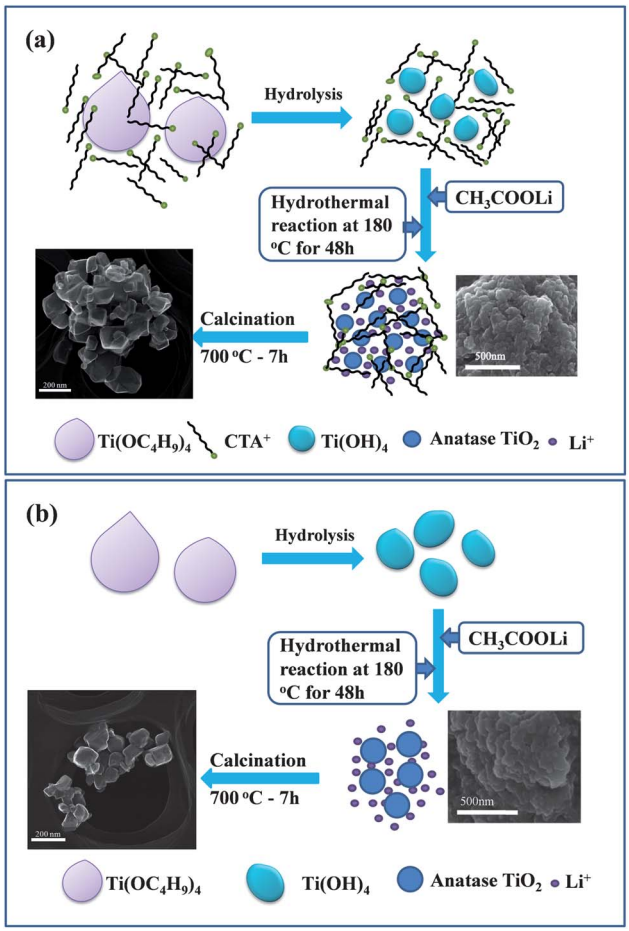

Fig. 1 Schematic illustration for synthesis of spinel $Li_4Ti_5O_{12}$ using (a) and without using (b) CTAB.

Structure characterization

The XRD patterns of the hydrothermal products (lithium acetate and $Ti(OH)_4$ as the hydrolysis products of $Ti(OC_4H_9)_4$) with and without CTAB are shown in Fig. 2a. It can be found that, for the hydrothermal products without CTAB, the peaks in the range between 25 and 90° can be indexed to the anatase TiO_2 (JCPDS card no. 21-1272). Peaks below 25° may be ascribed to the reactant lithium acetate (JCPDS card no. 14-0841) and the minor organic phases caused by the hydrolysis of $Ti(OC_4H_9)_4$. In the XRD patterns of the hydrothermal products prepared with CTAB, the peak around 21.5° sharpens greatly, which may be attributed to the long chain compounds polymerized by the hydrolysis products of $Ti(OC_4H_9)_4$ and decomposition products of CTAB. During the hydrothermal process, the $Ti(OH)_4$ derived from the hydrolysis of the $Ti(OC_4H_9)_4$ changed into anatase TiO_2, and other compounds such as the hydrolysis products and decomposition products of CTAB may be polymerized and change into long chain compounds.

After the hydrothermal products are calcined at 700 °C for 7 h in argon filled atmosphere, it can be seen from the XRD patterns of Fig. 2b that both samples exhibit good crystallinity and all diffraction peaks of the two samples are in accordance with spinel $Li_4Ti_5O_{12}$ (JCPDS card no. 49-0207). Though the hydrothermal products were calcined in argon filled atmosphere, no peaks for carbon and TiO_2 are detected in both $Li_4Ti_5O_{12}$/C samples with and without CTAB. Thus, this facile method results in pure $Li_4Ti_5O_{12}$/C composite.

The Raman spectra of the samples are examined to characterize the state of carbon. Fig. 2c shows the Raman spectra of $Li_4Ti_5O_{12}$/C synthesized in argon atmosphere. Two main bands are observed at around 1357 and 1597 cm^{-1} in the Raman spectra of $Li_4Ti_5O_{12}$/C, which are designated as the D band and G band, respectively. The G-peak corresponds to graphite in-plane vibrations with E_{2g} symmetry, and the D-peak is generally associated with a double-resonance effect. The value I_D/I_G (the peak intensity ratio) can be used to evaluate the degree of disorder for pyrolytic carbon.[36,37] The low values for the I_D/I_G parameter indicate a high degree of graphitization. The values of the I_D/I_G for $Li_4Ti_5O_{12}$/C with and without CTAB are

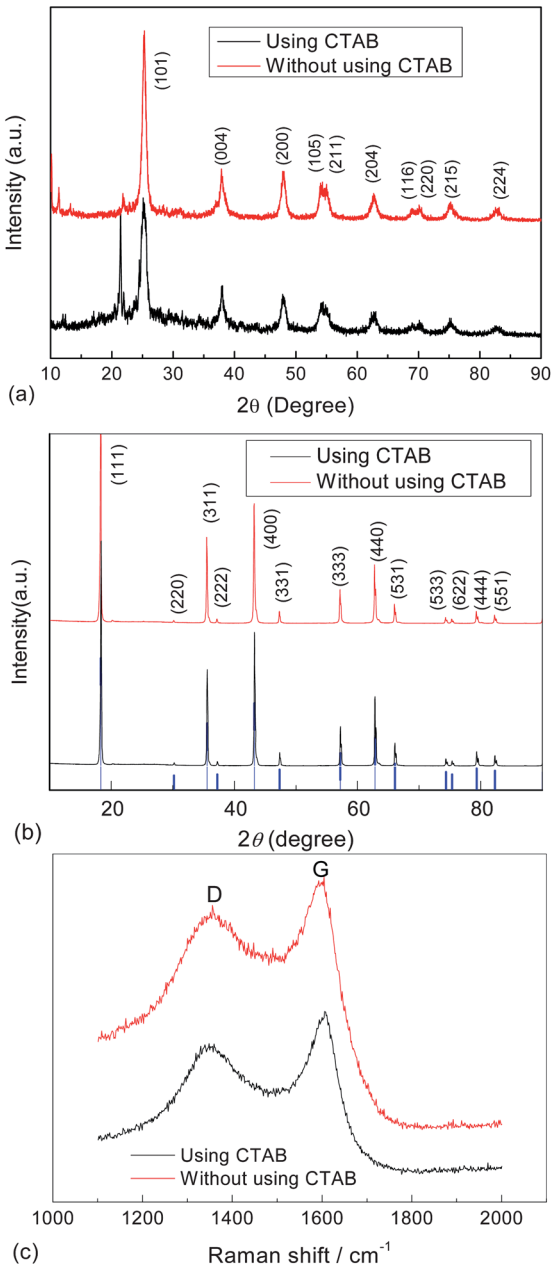

Fig. 2 XRD patterns of hydrothermal products of $Ti(OH)_4$ and lithium acetate before (a) and after (b) heat treatment at 700 °C for 7 h; Raman spectra of $Li_4Ti_5O_{12}$/C composite with and without CTAB (c).

respectively 2.04 and 2.15, which suggests that the carbon is mainly in amorphous state.

TEM characterization

TEM images of the $Li_4Ti_5O_{12}$/C with and without CTAB are shown in Fig. 3. Both samples show well crystallized particles. However, we can mainly find two differences about the samples with and without CTAB. First difference is the particle size. The grain size of sample with CTAB is about 70–200 nm, which is obviously larger than that without CTAB (60–120 nm). This is attributed to the fact that the hydrothermal products are covered by the long chain organics, which attach many primary TiO_2 particles together to form larger secondary TiO_2 particles as shown in Fig. 1a. Note that the anatase TiO_2 produced without CTAB has a relatively larger primary size, though it has a smaller secondary particle size. The secondary particles of TiO_2 react with Li ions to form $Li_4Ti_5O_{12}$/C composite particles during calcination. Thus, the particle size of $Li_4Ti_5O_{12}$/C with CTAB is larger than that without CTAB.

TEM images of $Li_4Ti_5O_{12}$ as shown in Fig. 3 indicate that the $Li_4Ti_5O_{12}$ powder has a cubic structural morphology. From the high resolution TEM images (Fig. 3b and d), it can be identified that the $Li_4Ti_5O_{12}$ particles with CTAB are coated uniformly with a thin carbon layer with thickness ~1 nm. For the $Li_4Ti_5O_{12}$/C sample without CTAB, the $Li_4Ti_5O_{12}$ particles are covered by relatively thick surface layers with thickness of ~2.5 nm (see Fig. 3d) and the carbon layers are not uniformly coated on the $Li_4Ti_5O_{12}$ particles. Consistently, the carbon content of the $Li_4Ti_5O_{12}$/C sample with CTAB is ~1.2 wt% and that of $Li_4Ti_5O_{12}$/C sample without CTAB is ~2.6 wt% by thermogravimetric (TG) measurements (see Fig. S1†).

Electrochemical characterization

The electrochemical performance of the prepared $Li_4Ti_5O_{12}$/C with and without CTAB was systematically investigated using the coin cells. Fig. 4a and b shows the rate charge and discharge performance of $Li_4Ti_5O_{12}$/C with and without CTAB, respectively. It can be found that the $Li_4Ti_5O_{12}$/C with CTAB exhibits much higher capacity than the $Li_4Ti_5O_{12}$/C without CTAB. A specific discharge capacity of 176 mA h g^{-1} is observed when the $Li_4Ti_5O_{12}$/C with CTAB is discharged at 0.1 C and that using the charge and discharge rate of 0.5, 1, 5 and 10 C is 166, 163, 156 and 151 mA h g^{-1}, respectively. Even using a charge and discharge rate as high as 20 C, the electrode can still deliver a specific capacity of 136 mA h g^{-1} and this value is about 77% of the capacity at 0.1 C, whereas the $Li_4Ti_5O_{12}$/C without CTAB can only deliver a reversible discharge capacity of 143 mA h g^{-1} at the discharge rate of 0.1 C, and capacities reduced to 114, 96, 69, 47 mA h g^{-1} at discharge rates of 0.5 C, 1 C, 5 C and 10 C, respectively. This indicates that the introduction of CTAB in the synthesis of $Li_4Ti_5O_{12}$/C greatly improves the rate discharge performance of $Li_4Ti_5O_{12}$/C. The concentration of CTAB solution employed in this work is 13 g L^{-1}, which is close to the saturation concentration of CTAB aqueous solution. According to our preliminary results, the CTAB concentrations is a key factor influencing the performance of the prepared $Li_4Ti_5O_{12}$/C and 13 g L^{-1} is an optimum concentration for CTAB employed in this work. The electrochemical performance of $Li_4Ti_5O_{12}$/C prepared using 13 g L^{-1} CTAB is much better than those using lower concentrations of CTAB (the case using 6.5 g L^{-1} CTAB as a typical example is presented in Fig. S2†). The detailed work is ongoing to precisely correlate the CTAB concentration, carbon coating structure and electrochemical performance of the resulting composite.

Another interesting result is the significantly different rate discharge performance. It is well-known that the small particles can shorten the lithium ion diffusion channel and the carbon coating layers can improve the electronic conductivity of the $Li_4Ti_5O_{12}$ particles. Thus, the $Li_4Ti_5O_{12}$/C without CTAB, which has a smaller particle size and relatively thick carbon layers, is expected to have a better rate discharge performance. However, the

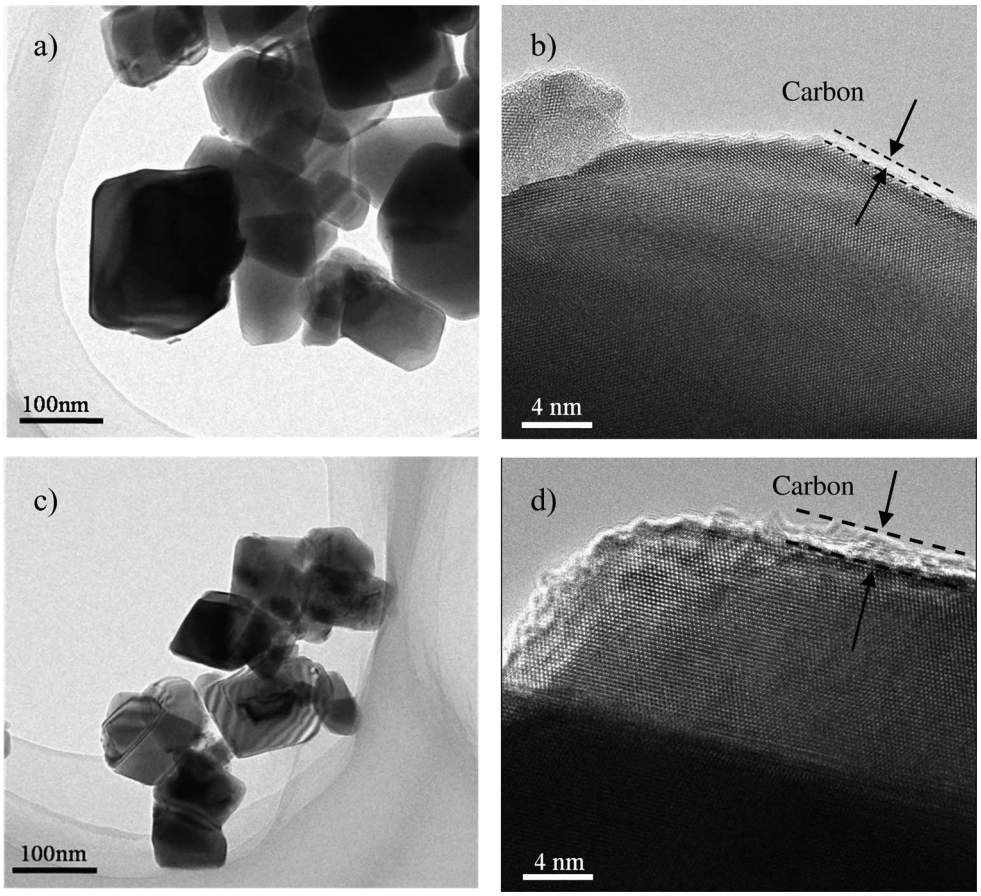

Fig. 3 TEM images of the $Li_4Ti_5O_{12}$/C using (a and b) and without using (c and d) CTAB.

$Li_4Ti_5O_{12}$/C with CTAB with larger particle size and relatively low carbon content show better rate charge and discharge performance. The CV and EIS of both $Li_4Ti_5O_{12}$/C composites were tested to explain why these two materials show such different performance.

It can be found from Fig. 4c that both samples have a couple redox peaks at around 1.46 and 1.68 V, which corresponds to the lithium ion intercalation and deintercalation of the spinel structure. The reduction and oxidation peaks below 0.6 V are caused by a multi-step restoration of Ti^{4+}.[38,39] The peak current density of $Li_4Ti_5O_{12}$/C with CTAB is much larger than that without CTAB. This suggests that the $Li_4Ti_5O_{12}$/C with CTAB possesses a higher rate performance. This result is consistent with that of Fig. 4a and b. The EIS of $Li_4Ti_5O_{12}$/C with and without CTAB is shown in Fig. 4d. The EIS was simulated by Z-view software using the equivalent circuit as shown in Fig. 4d. It can be observed that the experimental and simulated EIS are almost coincident. According to the equivalent circuit as shown in Fig. 4d, the intersection of the diagram with a real axis refers to a bulk resistance (R_b), which mainly reflects the resistance of electrode and electrolyte. The depressed semicircle from a high to medium frequency is attributed to the charge-transfer resistance (R_{ct}) and CPE1. Instead of a double-layer capacitance (C_{dl}), the constant phase element of CPE1 is used to take into account the roughness of the particle surface.[40–43] The slope line at low frequency corresponds to the Warburg impedance (Z_w), which is related to the lithium ion diffusion within the particles.

The simulation results shown in Table 2 show that the R_b of the $Li_4Ti_5O_{12}$/C with CTAB is 3.8 Ω, which is much larger than that (1.8 Ω) without CTAB. This suggests that the thick carbon coating can increase the electronic conductivity of particles, whereas it can be seen that the R_{ct} (19.2 Ω) of $Li_4Ti_5O_{12}$/C with CTAB is much less than that (50.2 Ω) without CTAB. This suggests that $Li_4Ti_5O_{12}$/C with CTAB has much larger Li ion conductivity which can also be confirmed by the following calculation of the lithium ion diffusion coefficient.

EIS is also an important tool for evaluating the diffusion coefficient of a lithium ion within the particles. The diffusion coefficient of the lithium ion is calculated according to the following equation:[44,45]

$$D_{Li} = \frac{R^2T^2}{2A^2n^4F^4C^2\sigma^2} \quad (1)$$

where D_{Li} represents the diffusion coefficient of the lithium ion, R is the gas constant, T the absolute temperature, A the surface area of electrode, n the number of electrons per molecule during oxidization, F the Faraday constant, C the concentration of lithium ion, and σ the Warburg factor, σ relates to Z' through eqn (2) and its value can be obtained from the slope of the lines between Z' and $\omega^{-1/2}$ as shown in Fig. 4f.

$$Z' = R_D + R_L + \sigma\omega^{-1/2} \quad (2)$$

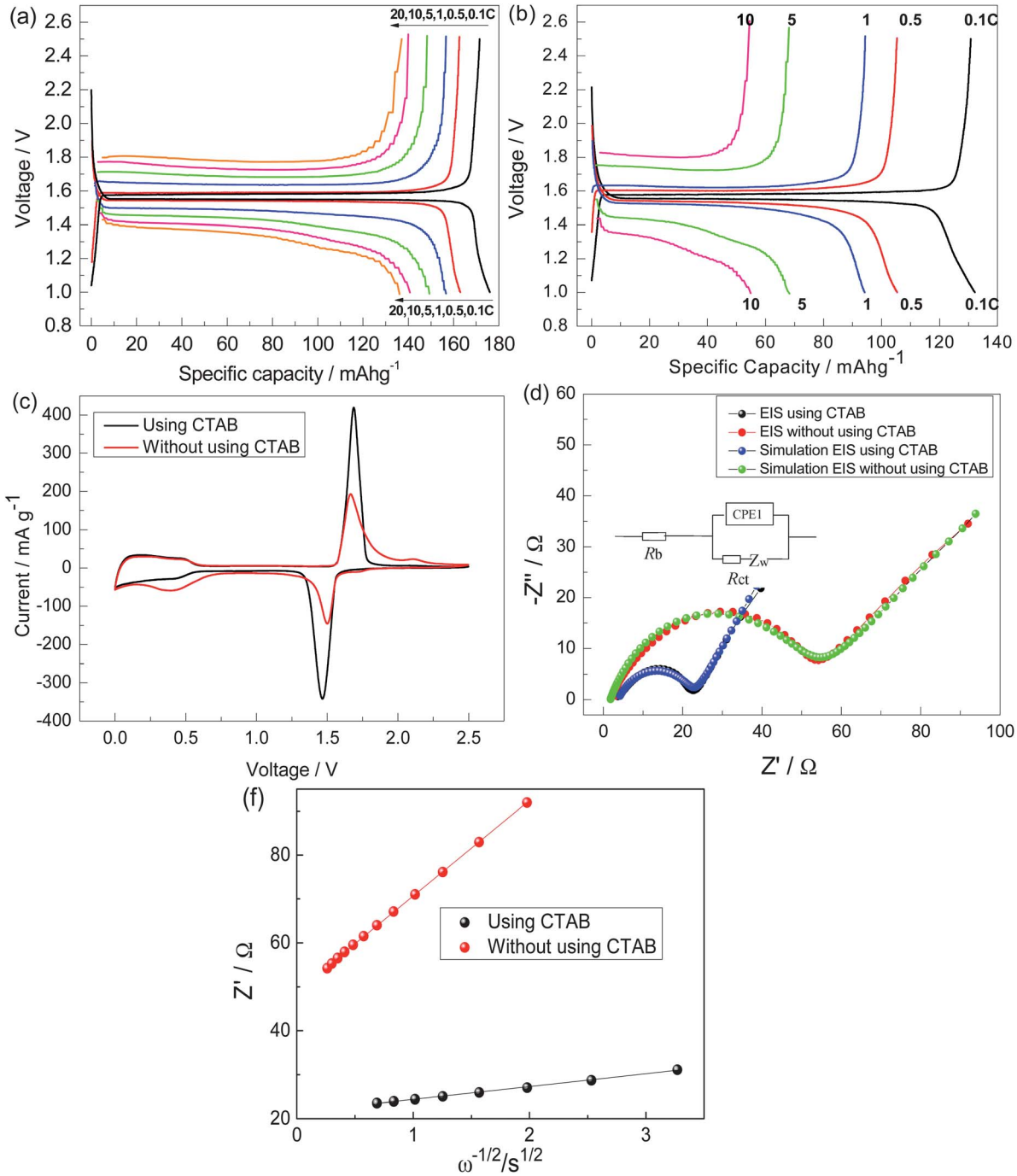

Fig. 4 Charge and discharge curves of $Li_4Ti_5O_{12}$/C with (a) and without (b) CTAB with a different charge and discharge rate; CV (c) and EIS (d) profiles of the obtained $Li_4Ti_5O_{12}$/C; real parts of the complex impedance *versus* $\omega^{-1/2}$ at $Li_4Ti_5O_{12}$/C 50% SOC (f).

Table 2 Simulation results of Fig. 4d

Samples	R_s (Ω)	R_{ct} (Ω)	σ	D_{Li} ($cm^2\ s^{-1}$)
Without CTAB	1.8	50.2	21.78	1.22×10^{-13}
With CTAB	3.8	19.2	2.92	6.82×10^{-12}

The diffusion coefficient of the lithium ion (D_{Li}) within the particles is calculated using eqn (1) and (2). It can be seen from Table 1 that the D_{Li} of the case with CTAB is larger by ~60 times than that without CTAB.

For the lithium ion intercalation and deintercalation reaction, the electrons and Li ions must reach or leave the reaction point in the active material simultaneously. R_{ct} depends on the electronic and ionic conductivity. Thus, the active material with an excellent rate charge and discharge performance must have both high electronic and ionic conductivity. The larger D_{Li} within the $Li_4Ti_5O_{12}$/C particles with CTAB suggests that the transport number of the lithium ion can satisfy the reaction requirement at

large charge and discharge current. In addition, for the $Li_4Ti_5O_{12}$/C without CTAB, the coated carbon layers may be too thick, thereby blocking the lithium ion diffusion and leading to poor ionic conductivity. Therefore, although the coated carbon layers can improve the electronic conductivity of the material, its ionic conductivity cannot satisfy the rapid electrochemical reaction.

The cycling performance of $Li_4Ti_5O_{12}$/C with and without CTAB is tested to examine the cycling stability at very high charge and discharge rates. It is seen from Fig. 5 that the initial discharge capacities of the $Li_4Ti_5O_{12}$/C with CTAB at 10 and 20 C (the charge and discharge rates are the same) are 150.2 and 134.9 mA h g^{-1}, respectively, and the retained discharge capacities after 200 cycles are 120.6 and 102.3 mA h g^{-1}. The capacity retention ratios for 10 and 20 C are 80.3 and 75.8%, respectively. It is well-known that the R_{ct} of coin cells is greatly larger than that of a commercial battery. That is, even for the coin cells, the above material shows excellent cycling performance at high rates (10 and 20 C). In addition, it can be found that the coloumbic efficiency of the material during cycling is ~100%. In contrast, for the $Li_4Ti_5O_{12}$/C without CTAB, the specific discharge capacities are only 51 and 41 mA h g^{-1}, respectively, at 10 C and 20 C, which are too small for the lithium ion batteries.

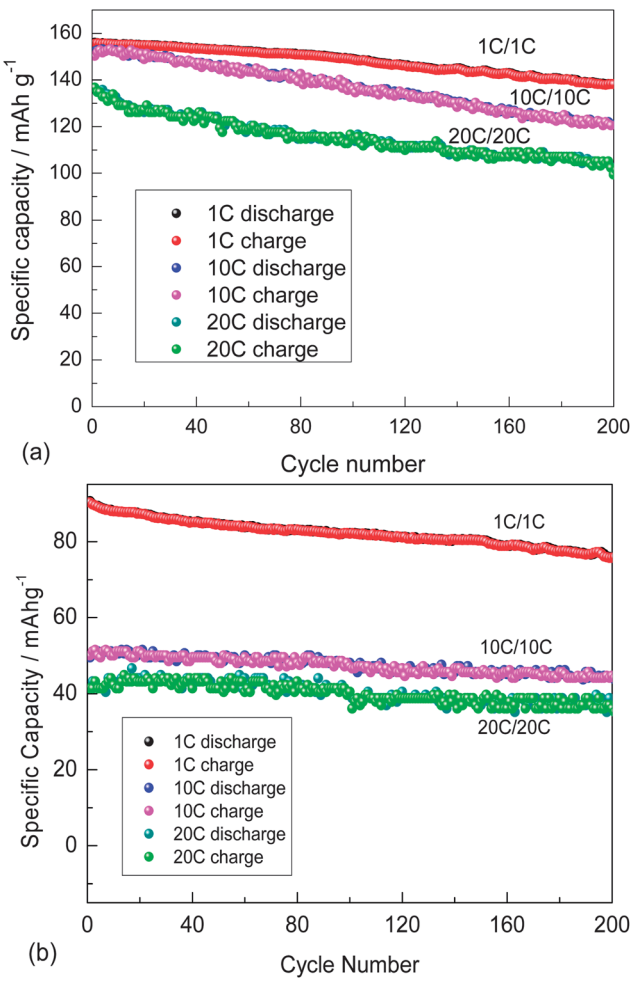

Fig. 5 Cycling performance of $Li_4Ti_5O_{12}$/C with (a) and without (b) CTAB at different charge and discharge rates.

Conclusions

We have successfully prepared a novel spinel $Li_4Ti_5O_{12}$/C composite with a lump morphology and excellent rate performance by a facile hydrothermal process followed by a low temperature heat treatment. The introduction of CTAB as a surfactant in the preparation significantly improves the rate performance of $Li_4Ti_5O_{12}$/C composite, which can deliver 151 and 136 mA h g^{-1} at a charge and discharge rate of 10 and 20 C, respectively. The excellent rate performance is attributed to the larger ion diffusion coefficient (6.82×10^{-12} cm^2 s^{-1}) and smaller charge-transfer resistance (R_{ct}) (19.2 Ω) for the $Li_4Ti_5O_{12}$/C prepared in presence of CTAB as compared to the case without CTAB (1.22×10^{-13} cm^2 s^{-1} and 50.2 Ω).

Acknowledgements

This work was supported by the National Nature Science Foundation of China (no. 51072131, 51202121 and 51232005) and the Key Project for Basic Research for three main areas of Shenzhen (no. JC201104210152A), Guangdong Province Innovation R&D Team Plan for Energy and Environmental Materials (no. 2009010025).

References

1 N. Yabuuchi, Y. Makimura and T. Ohzuku, *J. Electrochem. Soc.*, 2007, **154**, A314–A321.
2 J. M. Tarascon and M. Armand, *Nature*, 2001, **414**, 359–367.
3 M. Armand and J.-M. Tarascon, *Nature*, 2008, **451**, 652–657.
4 K. Amine, I. Belharouak, Z. Chen, T. Tran, H. Yumoto, N. Ota, S.-T. Myung and Y.-K. Sun, *Adv. Mater.*, 2010, **22**, 3052–3057.
5 E. Ferg, R. J. Gummow, A. de Kock and M. M. Thackeray, *J. Electrochem. Soc.*, 1994, **141**, L147–L150.
6 T. Ohzuku, A. Ueda and N. Yamamoto, *J. Electrochem. Soc.*, 1995, **142**, 1431–1435.
7 F. Ronci, P. Reale, B. Scrosati, S. Panero, V. R. Albertini, M. di Michiel, P. Perfetti and J. M. Merino, *J. Phys. Chem. B*, 2002, **106**, 3082–3086.
8 B. K. Guo, J. Shu, K. Tang, Y. Bai, Z. X. Wang and L. Q. Chen, *J. Power Sources*, 2008, **177**, 205–210.
9 X. Li, H. Zhu, K. Wang, A. Cao, J. Wei, C. Li, Y. Jia, Z. Li, X. Li and D. Wu, *Adv. Mater.*, 2010, **22**, 2743–2748.
10 B. Markovsky, F. Amalraj, H. E. Gottlieb, Y. Gofer, S. K. Martha and D. Aurbach, *J. Electrochem. Soc.*, 2010, **157**, A423–A429.
11 K. Zaghib, M. Simoneau, M. Armand and M. Gauthier, *J. Power Sources*, 1999, **82**, 300–305.
12 L. F. Shen, C. Z. Yuan, H. J. Luo, X. G. Zhang, L. Chen and H. S. Li, *J. Mater. Chem.*, 2011, **21**, 14414–14416.
13 Y. Tang, L. Yang, S. Fang and Z. Qiu, *Electrochim. Acta*, 2009, **54**, 6244–6249.
14 Y. F. Tang, L. Yang, Z. Qiu and J. S. Huang, *Electrochem. Commun.*, 2008, **10**, 1513–1516.
15 J. Chen, L. Yang, S. Fang and Y. Tang, *Electrochim. Acta*, 2010, **55**, 6596–6600.
16 S. H. Yu, A. Pucci, T. Herntrich, M. G. Willinger, S. H. Baek, Y. E. Sung and N. Pinna, *J. Mater. Chem.*, 2011, **21**, 806–810.
17 C. Lai, Y. Y. Dou, X. Li and X. P. Gao, *J. Power Sources*, 2010, **195**, 3676–3679.
18 K. Naoi, S. Ishimoto, Y. Isobe and S. Aoyagi, *J. Power Sources*, 2010, **195**, 6250–6254.
19 H. K. Kim, S. M. Bak and K. B. Kim, *Electrochem. Commun.*, 2010, **12**, 1768–1771.
20 L. F. Shen, C. Z. Yuan, H. J. Luo, X. G. Zhang, K. Xu and F. Zhang, *J. Mater. Chem.*, 2011, **21**, 761–767.
21 B. Li, F. Ning, Y.-B. He, H. Du, Q.-H. Yang, J. Ma, F. Kang and C.-T. Hsu, *Int. J. Electrochem. Sci.*, 2011, **6**, 3210–3223.
22 H. G. Jung, S. T. Myung, C. S. Yoon, S. B. Son, K. H. Oh, K. Amine, B. Scrosati and Y. K. Sun, *Energy Environ. Sci.*, 2011, **4**, 1345–1351.

23 L. F. Shen, X. G. Zhang, E. Uchaker, C. Z. Yuan and G. Z. Cao, *Adv. Energy Mater.*, 2012, **2**, 691–698.
24 Y. G. Wang, H. M. Liu, K. X. Wang, H. Eiji, Y. R. Wang and H. S. Zhou, *J. Mater. Chem.*, 2009, **19**, 6789–6795.
25 G.-N. Zhu, H.-J. Liu, J.-H. Zhuang, C.-X. Wang, Y.-G. Wang and Y.-Y. Xia, *Energy Environ. Sci.*, 2011, **4**, 4016–4022.
26 L. Zhao, Y. Hu, H. Li, Z. Wang and L. Chen, *Adv. Mater.*, 2011, **23**, 1385–1388.
27 Y. Q. Wang, L. Gu, Y. G. Guo, H. Li, X. Q. He, S. Tsukimoto, Y. Ikuhara and L. J. Wan, *J. Am. Chem. Soc.*, 2012, **134**, 7874–7879.
28 B. L. Cushing, V. L. Kolesnichenko and C. J. O'Connor, *Chem. Rev.*, 2004, **104**, 3893–3946.
29 V. Berry, A. Gole, S. Kundu, C. J. Murphy and R. F. Saraf, *J. Am. Chem. Soc.*, 2005, **127**, 17600–17601.
30 T. K. Sau and C. J. Murphy, *J. Am. Chem. Soc.*, 2004, **126**, 8648–8649.
31 C. J. Murphy, A. M. Gole, J. W. Stone, P. N. Sisco, A. M. Alkilany, E. C. Goldsmith and S. C. Baxter, *Acc. Chem. Res.*, 2008, **41**, 1721–1730.
32 M.-H. Lee, T.-H. Kim, Y. S. Kim and H.-K. Song, *J. Phys. Chem. C*, 2011, **115**, 12255–12259.
33 N. Du, Y. Xu, H. Zhang, J. Yu, C. Zhai and D. Yang, *Inorg. Chem.*, 2011, **50**, 3320–3324.
34 H. Kim and J. Cho, *Chem. Mater.*, 2008, **20**, 1679–1681.
35 Z. Sun, J. H. Kim, Y. Zhao, F. Bijarbooneh, V. Malgras, Y. Lee, Y.-M. Kang and S. X. Dou, *J. Am. Chem. Soc.*, 2011, **133**, 19314–19317.
36 X. B. Hu, Z. J. Lin, K. R. Yang, Y. J. Huai and Z. H. Deng, *Electrochim. Acta*, 2011, **56**, 5046–5053.
37 T. Yuan, X. Yu, R. Cai, Y. K. Zhou and Z. P. Shao, *J. Power Sources*, 2010, **195**, 4997–5004.
38 H. Ge, N. Li, D. Y. Li, C. S. Dai and D. L. Wang, *Electrochem. Commun.*, 2008, **10**, 719–722.
39 H. Ge, N. Li, D. Y. Li, C. S. Dai and D. L. Wang, *J. Phys. Chem. C*, 2009, **113**, 6324–6326.
40 F. Nobili, R. Tossici, F. Croce, B. Scrosati and R. Marassi, *J. Power Sources*, 2001, **94**, 238–241.
41 F. Croce, F. Nobili, A. Deptula, W. Lada, R. Tossici, A. D'Epifanio, B. Scrosati and R. Marassi, *Electrochem. Commun.*, 1999, **1**, 605–608.
42 M. Umeda, K. Dokko, Y. Fujita, M. Mohamedi, I. Uchida and J. R. Selman, *Electrochim. Acta*, 2001, **47**, 885–890.
43 G. T. K. Fey, W. H. Yo and Y. C. Chang, *J. Power Sources*, 2002, **105**, 82–86.
44 N. Takami, A. Satoh, M. Hara and T. Ohsaki, *J. Electrochem. Soc.*, 1995, **142**, 371–379.
45 S.-L. Chou, J.-Z. Wang, H.-K. Liu and S.-X. Dou, *J. Phys. Chem. C*, 2011, **115**, 16220–16227.

